The 'Lorenz' grid computational mode: implications for transparent boundary conditions and vertical two grid noise.

A McDonald

Met Éireann, Dublin, Ireland.

Corresponding author address:

Aidan McDonald, Met Éireann, Glasnevin Hill, Dublin 9, Ireland.

E-mail: aidan.mcdonald@met.ie

ABSTRACT

Using the Lorenz grid to discretize in the vertical creates difficulties for data analysis, initialization, numerical weather prediction and transparent boundary conditions. An alternative discretization is proposed, and some of its implications for transparent boundary conditions and numerical weather prediction are examined.

1. Introduction.

A problem arises with the 'Lorenz' (1960) vertical discretization scheme if one needs to regenerate the temperature (T) and surface pressure (p_s) fields from the geopotential height (Φ) fields: the equation relating them is under determined. In the past this problem has surfaced in data analysis, initialization, and numerical weather prediction. Conventionally, an ad-hoc additional condition, which is physically reasonable, is invoked to overcome this obstacle. For example, Hoskins and Simmons (1975), in integrating their global spectral semi-implicit model, chose p_s such that the amplitude of the vertical two grid structure in T is minimised. See also 'step c' on page 108 of Daley (1979) for his physical assumption, made in the context of normal mode initialization. More recently, it has been an obstacle to the development of transparent boundary conditions; see McDonald (2006).

Hollingsworth (1995) examined this problem and suggested using a Charney-Phillips (1953) vertical discretization scheme instead. Although this eliminates the difficulty it is unattractive to Lorenz grid users because it involves a complete re-coding of the dynamical equations of motion. The purpose of this note is to show that the undetermined relationship between T, p_s and Φ characteristic of the Lorenz grid can be eliminated by making a minor change to the Lorenz scheme. In contrast to the major re-coding required for a switch to the Charney-Phillips grid, only minor code changes are needed for its implementation.

An additional, related, aspect of the Lorenz discretization is that the equations of motion support a spurious computational mode; see Hollingsworth (1995) for a discussion. He makes the point that its presence could lead to the growth of a vertical two grid wave in the temperature field which, in turn, could cause spurious convection and rainfall.

In section 2 the σ model equations are solved in two dimensions ($x - \sigma$) using the Lorenz discretization in the vertical. The purpose is two-fold. First, to illustrate these two problems associated with the Lorenz grid. Second, to contrast their solution (a) on a 'tweaked' the Lorenz grid, and (b) on the Charney-Phillips grid.

In section 3 it is demonstrated that reconstruction of T and lnp_s from Φ is essential

for building transparent boundary conditions, which excludes using the Lorenz grid. It is shown how the 'tweaked Lorenz' grid overcomes this impasse. In section 4 is shown how to program the HIRLAM dynamics using the 'tweaked Lorenz' grid and a demonstration forecast is performed.

Eliminating the spurious mode raises the possibility of reducing vertical two grid noise. Section 5 contains a discussion of this issue along with an additional suggestion for addressing this problem.

2. The sigma model

2.1 The equations of motion

The linearized inviscid hydrostatic primitive equations in σ co-ordinates (Phillips, 1957) can be written as follows.

$$\frac{du}{dt} + \frac{\partial G}{\partial x} - fv = 0, \tag{2.1.1}$$

$$\frac{dv}{dt} + \frac{\partial G}{\partial y} + fu = 0, \tag{2.1.2}$$

$$\frac{dlnp_s}{dt} + D + \frac{\partial \dot{\sigma}}{\partial \sigma} = 0, \tag{2.1.3}$$

$$\frac{dT}{dt} - \frac{RT^0}{C_p}\left(\frac{dlnp_s}{dt} + \frac{\dot{\sigma}}{\sigma}\right) = 0, \tag{2.1.4}$$

$$\frac{\partial \Phi}{\partial \sigma} + \frac{RT}{\sigma} = 0, \tag{2.1.5}$$

where

$$G = \Phi + RT^0 lnp_s, \qquad D = \frac{\partial u}{\partial x} + \frac{\partial v}{\partial y}, \tag{2.1.6}$$

and

$$\frac{d}{dt} = \frac{\partial}{\partial t} + u^0\frac{\partial}{\partial x} + v^0\frac{\partial}{\partial y}. \tag{2.1.7}$$

In these equations $\sigma = p/p_s$ where p is the pressure and p_s is the surface pressure. At the surface $\sigma = 1$ by definition. The top of the atmosphere is at $\sigma = \sigma_T$. The horizontal velocities in the easterly and northerly directions are u and v, respectively, Φ is the geopotential height, T is the temperature and $\dot{\sigma}$ is the vertical velocity. The temperature T^0 is constant, $R = 287.04$ J kg^{-1}K^{-1} is the gas constant for dry air, and $C_p = 1004.64$ J kg^{-1}K^{-1} is its specific heat at constant pressure; u^0 and v^0 are constants.

At the top and bottom of the atmosphere the vertical velocities are assumed to be zero:

$$\dot{\sigma}(\sigma_T) = 0; \qquad \dot{\sigma}(1) = 0. \tag{2.1.8}$$

2.2 Vertical discretization

Discretizing in the vertical using the Lorenz-grid, see table 1, gives for eqs. (2.1.1)-(2.1.5)

$$\frac{du_m}{dt} + \frac{\partial G_m}{\partial x} - fv_m = 0, \tag{2.2.1}$$

$$\frac{dv_m}{dt} + \frac{\partial G_m}{\partial y} + fu_m = 0, \tag{2.2.2}$$

$$\frac{dlnp_s}{dt} + D_m + \frac{\dot{\sigma}_{m+\frac{1}{2}} - \dot{\sigma}_{m-\frac{1}{2}}}{\Delta\sigma_m} = 0, \tag{2.2.3}$$

$$\frac{dT_m}{dt} - \frac{RT^0}{2C_p\sigma_m}\Big(\sigma_{m+\frac{1}{2}}\frac{dlnp_s}{dt} + \dot{\sigma}_{m+\frac{1}{2}} + \sigma_{m-\frac{1}{2}}\frac{dlnp_s}{dt} + \dot{\sigma}_{m-\frac{1}{2}}\Big) = 0, \tag{2.2.4}$$

$$\frac{\Phi_{m+\frac{1}{2}} - \Phi_{m-\frac{1}{2}}}{\Delta\sigma_m} + \frac{RT_m}{\sigma_m} = 0, \tag{2.2.5}$$

where $m = 1, M$ and, by definition

$$\sigma_m = (\sigma_{m+\frac{1}{2}} + \sigma_{m-\frac{1}{2}})/2; \qquad \Delta\sigma_m = \sigma_{m+\frac{1}{2}} - \sigma_{m-\frac{1}{2}}. \tag{2.2.6}$$

Summing eq. (2.2.3) from top to bottom and using eq. (2.1.8) yields

$$\frac{dlnp_s}{dt} = -\frac{1}{(1-\sigma_T)}\sum_{j=1}^{M}\Delta\sigma_j D_j \equiv -\boldsymbol{\nu.D}. \tag{2.2.7}$$

A partial sum of eq. (2.2.3) from the top down, using eqs. (2.1.8) and (2.2.7) yields

$$\dot{\sigma}_{m+\frac{1}{2}} = \Big(\frac{\sigma_{m+\frac{1}{2}} - \sigma_T}{1-\sigma_T}\Big)\sum_{j=1}^{M}\Delta\sigma_j D_j - \sum_{j=1}^{m}\Delta\sigma_j D_j, \tag{2.2.8}$$

which, when combined with eq. (2.2.7) and substituted in eq. (2.2.4), gives

$$\frac{dT_m}{dt} = -\frac{RT^0}{C_p\sigma_m}\Big(\frac{\sigma_T}{1-\sigma_T}\sum_{j=1}^{M}\Delta\sigma_j D_j + \frac{\Delta\sigma_m}{2}D_m + \sum_{j=1}^{m-1}\Delta\sigma_j D_j\Big) \equiv -(\boldsymbol{\tau D})_m. \tag{2.2.9}$$

Lastly, summing eq. (2.2.5) from the bottom up and using eq. (2.1.6) gives

$$G_m = \Phi_{M+\frac{1}{2}} + RT^0 lnp_s + R\Big(\frac{\Delta\sigma_m}{2\sigma_m}T_m + \sum_{j=m+1}^{M}\frac{\Delta\sigma_j}{\sigma_j}T_j\Big) = \Phi_{M+\frac{1}{2}} + RT^0 lnp_s + (\boldsymbol{\gamma T})_m. \tag{2.2.10}$$

2.3 Solution of the vertically discretized equations

Substituting

$$\psi_m(x,y,t) = \hat{\psi}_m exp[i(kx + ly - \omega t)] \tag{2.3.1}$$

for each of the fields u, v, T, G and $lnp_s(x,y,t) = \hat{l}\ exp[i(kx + ly - \omega t)]$ in eqs. (2.2.1), (2.2.2), (2.2.9), (2.2.7) and (2.2.10) gives, in the absence of orography,

$$-i\Omega\hat{u}_m + ik\hat{G}_m - f\hat{v}_m = 0, \tag{2.3.2}$$

$$-i\Omega\hat{v}_m + il\hat{G}_m + f\hat{u}_m = 0, \tag{2.3.3}$$

$$-\Omega\hat{T}_m + \sum_{j=1}^{M} \tau_{m,j}(k\hat{u}_j + l\hat{v}_j) = 0, \tag{2.3.4}$$

$$-\Omega\hat{l} + \sum_{j=1}^{M} \nu_{m,j}(k\hat{u}_j + l\hat{v}_j) = 0, \tag{2.3.5}$$

$$\hat{G}_m = RT^0\hat{l} + \sum_{j=1}^{M} \gamma_{m,j}\hat{T}_j, \tag{2.3.6}$$

where $-\Omega = -\omega + ku^0 + lv^0$. Combining eqs. (2.3.2) and (2.3.3) gives

$$\hat{u}_m = \frac{k\Omega + ilf}{\Omega^2 - f^2}\hat{G}_m; \qquad \hat{v}_m = \frac{l\Omega - ikf}{\Omega^2 - f^2}\hat{G}_m, \tag{2.3.7}$$

which when substituted in eqs. (2.3.4) and (2.3.5) combined with eq. (2.3.6), gives the following well-known result:

$$\Omega[(\Omega^2 - f^2)\mathbf{I} - (k^2 + l^2)\mathbf{M}]\hat{\mathbf{G}} = 0, \tag{2.3.8}$$

where

$$\mathbf{M} = RT^0\boldsymbol{\nu}. + \boldsymbol{\gamma\tau}\ . \tag{2.3.9}$$

If there exists a matrix $\mathbf{E}$, which diagonalises $\mathbf{M}$ and those diagonal elements are called λ_j, then eq. (2.3.8) can be re-written as

$$\Omega[(\Omega^2 - f^2) - (k^2 + l^2)\lambda_j](\mathbf{E^{-1}}\hat{\mathbf{G}})_j = 0, \tag{2.3.10}$$

which has $2M$ 'gravity wave solutions' for which Ω is given by

$$\Omega^j_{\pm} = \pm\sqrt{(k^2 + l^2)\lambda_j + f^2}, \tag{2.3.11}$$

and M 'slow' or 'advection' solutions for which $\Omega_a^j = 0$. For the gravity waves there is no problem: for instance, the solution associated with Ω_+^j is $\hat{G}_{+m}^j exp[i(kx + ly - \omega_+^j t)]$ and the associated $\hat{u}, \hat{v}, \hat{T}$ and $\hat{l}$ follow from eqs. (2.3.7), (2.3.4) and (2.3.5), respectively.

On the other hand, there is a problem with the advective solution. Given the solution $\hat{G}_{am}^j exp[i(kx+ly-\omega_a^j t)]$, $\hat{u}$ and $\hat{v}$ follow from eq. (2.3.7), but because $\Omega_a^j = 0$, eqs. (2.3.4) and (2.3.5) yield no information about $\hat{T}$ or $\hat{l}$. There remains eq. (2.3.6), which can be inverted to give

$$\hat{T}_m + RT^0\hat{l}(\boldsymbol{\gamma^{-1}I}\ )_m = (\boldsymbol{\gamma^{-1}\hat{G}}\ )_m. \tag{2.3.12}$$

This is under determined: given M values of $\hat{G}$, it is not possible to extract $M + 1$ quantities: $\hat{l}$, plus M values of $\hat{T}_m$.

Thus, the system of equations (2.3.2)-(2.3.6) supports an advective solution which could, for example, have physically reasonable values of $\hat{\mathbf{G}}, \hat{\mathbf{u}}, \hat{\mathbf{v}}$ and physically ridiculous values of $\hat{\mathbf{T}}$ and $\hat{l}$ such that eq. (2.3.12) was still satisfied. This is a well-known problem associated with this vertical discretization and, as was mentioned in the introduction, an additional ad-hoc assumption is needed to solve eq. (2.3.12).

2.4 Elimination of the spurious mode: Lorenz grid tweaked.

The purpose of this section is to describe a method of eliminating the spurious computational mode described in section 2.3 *without proposing a full re-coding of the dynamics.* In fact, as will be seen, all that is required is a redefinition of the matrix $\boldsymbol{\gamma}$ and a single row of the matrix $\boldsymbol{\tau}$ This is accomplished by replacing eqs. (2.2.4) and (2.2.5) with

$$\frac{dT_m}{dt} - \frac{RT^0}{2C_p\sigma_m}\left(\sigma_{m+\frac{1}{2}}\frac{dlnp_s}{dt} + \dot{\sigma}_{m+\frac{1}{2}} + \sigma_{m-\frac{1}{2}}\frac{dlnp_s}{dt} + \dot{\sigma}_{m-\frac{1}{2}}\right) = 0; \quad m = 1, M; \quad m \neq K, \tag{2.4.1}$$

$$\frac{\Phi_{m+\frac{1}{2}} - \Phi_{m-\frac{1}{2}}}{\Delta\sigma_m} + \frac{RT_m}{\sigma_m} = 0: \quad m = 1, M; \quad m \neq K \tag{2.4.2}$$

and

$$\frac{\Phi_{K+\frac{1}{2}} - \Phi_{K-\frac{1}{2}}}{\Delta\sigma_K} + \frac{R(T_{K+1} + T_{K-1})}{2\sigma_K} = 0. \tag{2.4.3}$$

Notice there is no temperature field T_K. The logic is that the relationship formerly given by eq. (2.2.10) will now have M fields on the right hand side of the equation instead of

$M+1$. The dropped level, K, can be any except levels 1 or M. Either of these could, of course, be dropped provided an extrapolation is used to compute the temperature T_1 or T_M in the equivalent of eq. (2.4.3).

The result of these changes is that G_m, instead of being defined by eq. (2.2.10) is now defined by

$$G_m = \Phi_{M+\frac{1}{2}} + RT^0 lnp_s + (\boldsymbol{\gamma}\overline{\boldsymbol{T}})_m, \tag{2.4.4}$$

where

$$\overline{T}_m = T_m \quad m \neq K; \qquad \overline{T}_K = (T_{K+1} + T_{K-1})/2. \tag{2.4.5}$$

It is useful to get eq. (2.4.4) into $M \times M$ matrix format. To do so, notice that since the temperature at level K is given by eq. (2.4.5), the *vector element* T_K is available to be defined as

$$T_K = T^0 lnp_s. \tag{2.4.6}$$

For reasons that will become obvious write

$$\overline{T}_K = (T_{K+1} - 2T_K + T_{K-1})/2 + T_K. \tag{2.4.7}$$

Then eq. (2.4.4) becomes

$$\begin{aligned} \mathbf{G} &= \Phi_{M+\frac{1}{2}}\mathbf{I} + RT_K\mathbf{I} + \boldsymbol{\gamma}\boldsymbol{T} + \boldsymbol{\gamma}(\overline{\boldsymbol{T}} - \boldsymbol{T}) \\ &= \Phi_{M+\frac{1}{2}}\mathbf{I} + \mathbf{c^K}\mathbf{T} + \boldsymbol{\gamma}\boldsymbol{T} + \boldsymbol{\gamma}\boldsymbol{r^K}\boldsymbol{T}\ . \end{aligned} \tag{2.4.8}$$

Since $\overline{T}_m - T_m = 0$ for all $m \neq K$, and from eq. (2.4.7), $\overline{T}_K - T_K = (T_{K+1} - 2T_K + T_{K-1})/2$, $\mathbf{r^K}$ is a matrix whose elements are all zero except $r^K_{K,K-1} = 0.5$, $r^K_{K,K} = 1$ and $r^K_{K,K+1} = 0.5$. Also, $\mathbf{c^K}$ is a matrix whose columns are all zero except for column K, all of whose elements equals R. Thus the relationship between $\mathbf{G}, \mathbf{T}$ and lnp_s is in an invertible form:

$$G_m = \Phi_{M+\frac{1}{2}} + (\check{\boldsymbol{\gamma}}\boldsymbol{T})_m; \qquad \check{\boldsymbol{\gamma}} = \boldsymbol{\gamma} + \boldsymbol{\gamma}\boldsymbol{r^K} + \mathbf{c^K}. \tag{2.4.9}$$

The temperature evolution equation can also be returned to square matrix form by taking d/dt of eq. (2.4.6) and substituting eq. (2.2.7):

$$\frac{dT_K}{dt} = -T^0\boldsymbol{\nu}.\boldsymbol{D}, \tag{2.4.10}$$

which means that

$$\frac{dT_m}{dt} = -(\check{\boldsymbol{\tau}}\boldsymbol{D})_m; \qquad m = 1, M, \tag{2.4.11}$$

where $\check{\boldsymbol{\tau}}$ is defined by the relationships

$$(\check{\boldsymbol{\tau}}\boldsymbol{D})_K = T^0(\boldsymbol{\nu}.\boldsymbol{D}), \qquad (\check{\boldsymbol{\tau}}\boldsymbol{D})_m = (\boldsymbol{\tau}\boldsymbol{D})_m; \quad m = 1, M; \quad m \neq K. \tag{2.4.12}$$

2.5 Implications of the 'tweaked Lorenz' grid.

The major implication is that, given $\mathbf{G}$, then $\mathbf{T}$ and lnp_s are uniquely defined via eqs. (2.4.9) and (2.4.6). By inference, the spurious mode is eliminated. This can be seen by substituting the solution eq. (2.3.1) in eqs. (2.4.11) and (2.4.9) with flat orography, resulting in

$$-\Omega\hat{T}_m + \sum_{j=1}^{M} \check{\tau}_{m,j}(k\hat{u}_j + l\hat{v}_j) = 0 \tag{2.3.4a}$$

and

$$\hat{G}_m = \sum_{j=1}^{M} \check{\gamma}_{m,j}\hat{T}_j. \tag{2.3.6a}$$

The derivation proceeds as in section 2.3, and the result is again given by eq. (2.3.8) with $\boldsymbol{M}$ now defined by

$$\mathbf{M} = \check{\boldsymbol{\gamma}}\check{\boldsymbol{\tau}} \ . \tag{2.3.9a}$$

As in section 2.3, there are still $2\times M$ gravity waves, but now there is no problem with the advective solutions: there are M of them only. Now, given the solution $\hat{G}^j_{am}exp[i(kx+ly-\omega^j_a t)]$, $\hat{u}$ and $\hat{v}$ follow from eq. (2.3.7), but importantly, in contrast to eq. (2.3.6), eq. (2.3.6a) can be inverted to give $\hat{T}_m$; $m = 1, M$. From that and eq. (2.4.6), $\hat{l} = \hat{T}_K/T^0$ follows: there is no spurious solution.

The other implications of the 'tweaked Lorenz' grid are that the eigenvalues and eigenvectors of $\mathbf{M}$ will be different. Are they degraded by the procedure? For example, with ten equally spaced σ levels and with $\sigma_T = 0.001$ and $T^0 = 250$K, the change in the gravity wave speeds, $c_k = \sqrt{\lambda_k}$ can be seen in table 2. The values of K are those which have the largest ($K = 8$) and smallest ($K = 2$) and an in-between ($K = 5$) value of c_{10}. As can be seen, there is good agreement for c_1, c_2, and c_3. However, $c_4(K = 2)$

differs from $c_4(K = 8)$ by approximately 5%. Is this significant? Almost certainly not because already the associated eigenvector is seriously in error for both the Lorenz and the 'tweaked Lorenz' grids; see fig. 1. Proceeding from c_5 to c_{10} the the associated eigenvectors become progressively less accurate, and, in fact, for the eigenvector associated with c_{10} the only correspondence between the coarse and fine mesh is the fact that each has nine nodes; see fig. 2.

mode	$c(Lor)$	$c(K = 2)$	$c(K = 5)$	$c(K = 8)$
1	312.22	312.20	312.25	312.23
2	163.14	163.14	163.22	163.13
3	78.08	77.99	77.86	78.11
4	43.73	41.72	43.09	43.68
5	27.43	24.75	26.87	27.00
6	18.21	15.76	17.48	17.54
7	12.33	10.25	10.27	12.26
8	8.23	6.44	7.97	7.70
9	5.11	3.49	4.68	3.37
10	2.54	0.90	1.30	2.54

TABLE 2. The gravity wave speeds for the a 10 level model with ten equally spaced σ levels and with $\sigma_T = 0.001$ and $T^0 = 250K$. Those for the Lorenz grid are in column 2, and those for the 'tweaked Lorenz' grid with $K = 2, 5, 8$ are in columns 3, 4 and 5, respectively.

2.6 Elimination of the spurious mode: Charney-Phillips grid.

Hollingsworth (1995) eliminated the spurious mode using the Charney-Phillips grid. The purpose of this section is to briefly discuss that option. For that grid, see table 1, the u, v and lnp_s equations are as in eqs. (2.2.1)-(2.2.3). The temperature equation is now

$$\frac{dT_{m+\frac{1}{2}}}{dt} - \frac{RT^0}{C_p\sigma_{m+\frac{1}{2}}}\left(\sigma_{m+\frac{1}{2}}\frac{dlnp_s}{dt} + \dot{\sigma}_{m+\frac{1}{2}}\right) = 0; \qquad m = 1, M-1, \tag{2.6.1}$$

which becomes, using eqs. (2.2.7) and (2.2.8),

$$\frac{dT_{m+\frac{1}{2}}}{dt} = -\frac{RT^0}{C_p\sigma_{m+\frac{1}{2}}}\left(\frac{\sigma_T}{1-\sigma_T}\sum_{j=1}^{M}\Delta\sigma_j D_j + \sum_{j=1}^{m}\Delta\sigma_j D_j\right) \qquad m = 1, M-1. \tag{2.6.2}$$

On this grid the hydrostatic equation becomes

$$\frac{\Phi_{m+\frac{3}{2}} - \Phi_{m-\frac{1}{2}}}{\sigma_{m+\frac{3}{2}} - \sigma_{m-\frac{1}{2}}} + \frac{RT_{m+\frac{1}{2}}}{\sigma_{m+\frac{1}{2}}} = 0; \qquad m = 1, M-1. \tag{2.6.3}$$

Because there are only $M-1$ equations here, and because only one of the $M+1$ values of Φ_m is known ($\Phi_{M+\frac{1}{2}}$) and additional equation is required. Thus, just as in the 'tweaked Lorenz' grid of section 2.4 it is necessary to introduce an alternative approximation for the hydrostatic equation at one of the levels. Hollingsworth (1995) assumed that the lowest layer was isothermal, which is equivalent to

$$\frac{\Phi_{M+\frac{1}{2}} - \Phi_{M-\frac{1}{2}}}{\sigma_{M+\frac{1}{2}} - \sigma_{M-\frac{1}{2}}} + \frac{RT_{M-\frac{1}{2}}}{\sigma_M} = 0, \tag{2.6.4}$$

that is, a zero order extrapolation of $T_{M-\frac{1}{2}}$ to level M. See also section 4 of Davies et al. (2005).

Summing eqs. (2.6.4) and (2.6.3) from the bottom up using G_m defined by eqs. (2.1.6) and (2.2.6) gives

$$G_m = \Phi_{M+\frac{1}{2}} + R\left(T^0 lnp_s + \frac{\Delta\sigma_M}{2\sigma_M}T_{M-\frac{1}{2}} + \sum_{j=m+1}^{M}\frac{\Delta\sigma_{j-\frac{1}{2}}}{\sigma_{j-\frac{1}{2}}}T_{j-\frac{1}{2}}\right) \tag{2.6.5}$$

where

$$\Delta\sigma_{j-\frac{1}{2}} = (\sigma_{j+\frac{1}{2}} - \sigma_{j-\frac{3}{2}})/2 \tag{2.6.6}$$

If the *vector elements* T^c_m are defined as

$$T^c_M = T^0 lnp_s; \qquad T^c_m = T_{m+\frac{1}{2}}, \quad m = 1, M-1, \tag{2.6.7}$$

then eq. (2.6.5) can be written as

$$G_m = \Phi_{M+\frac{1}{2}} + (\boldsymbol{\gamma^c T^c})_m, \tag{2.6.8}$$

where $\boldsymbol{\gamma^c}$ is an $M \times M$ matrix defined by eqs. (2.6.5)-(2.6.8). Also, the time evolution of $\boldsymbol{T^c}$ is given by

$$\frac{dT^c_m}{dt} = -(\boldsymbol{\tau^c D})_m; \qquad m = 1, M. \tag{2.6.9}$$

where $\boldsymbol{\tau^c}$ is an $M \times M$ matrix for which τ^c_M is defined by eqs. (2.6.7) and (2.2.7) and τ^c_m is defined by eqs. (2.6.7) and (2.6.2) for $m = 1, M-1$.

2.7 Discussion

Thus, for both the 'tweaked Lorenz' and Charney-Phillips grids, the spurious mode is eliminated by discretizing in the vertical such that T is defined at $M-1$ grid points if $\mathbf{v}$ is defined at M grid points. There is no inherent advantage in defining T at the 'half-levels' instead of the 'full levels'. In either case the temperature in one of the layers is determined by an extrapolation or interpolation of the temperature of the other layers. Of course, there may be other reasons for preferring the Charney-Phillips grid besides eliminating the spurious computational mode. For the arguments in favour see Arakawa and Konor (1996) and the references therein.

3. The 'tweaked Lorenz' grid and transparent boundary conditions.

3.1 Derivation of transparent boundary conditions

In the absence of orography transparent boundary conditions can be derived by first multiplying eq. (2.4.11) by $\check{\boldsymbol{\gamma}}$ to get

$$\frac{dG_m}{dt} + (\check{\boldsymbol{\gamma}}\check{\boldsymbol{\tau}}\boldsymbol{D})_m = 0; \qquad m = 1, M. \tag{3.1.1}$$

Assume there exists a matrix $\mathbf{E}$ which diagonalizes $\check{\boldsymbol{\gamma}}\check{\boldsymbol{\tau}}$:

$$\mathbf{E}^{-1}\check{\boldsymbol{\gamma}}\check{\boldsymbol{\tau}}\boldsymbol{E} \ = \mathbf{C^2}, \tag{3.1.2}$$

where the diagonal matrix has been written as $\mathbf{C^2}$. The diagonal elements are defined as $C_{m,m} = c_m$. By using eq. (3.1.2), equations (3.1.1), (2.2.1) and (2.2.2) can be re-written as

$$\frac{d(\mathbf{E^{-1}G})_m}{dt} + c_m^2(\mathbf{E^{-1}D})_m = 0, \tag{3.1.3}$$

$$\frac{d(\mathbf{E^{-1}u})_m}{dt} + \frac{\partial(\mathbf{E^{-1}G})_m}{\partial x} - f(\mathbf{E^{-1}v})_m = 0, \tag{3.1.4}$$

$$\frac{d(\mathbf{E^{-1}v})_m}{dt} + \frac{\partial(\mathbf{E^{-1}G})_m}{\partial y} + f(\mathbf{E^{-1}u})_m = 0, \tag{3.1.5}$$

For each $m = 1, M$ eqs. (3.1.3)-(3.1.5) with $\partial/\partial y = 0$ are formally identical to eqs. (79)-(81) of M06. Thus, the method of constructing transparent boundary conditions described in M06 is exactly what is required for the σ-model without further elaboration. Once the boundary conditions for $\mathbf{G}$, $\mathbf{u}$, and $\mathbf{v}$ have been derived those for $\mathbf{T}$ and lnp_s follow from eqs. (2.4.9) and (2.4.6), respectively.

Contrast this with the Lorenz grid. On it, deriving the transparent boundary conditions for $\mathbf{G}$, $\mathbf{u}$, and $\mathbf{v}$ follows exactly the same procedure. The insuperable difficulty is that it is not possible to extract a corresponding $\mathbf{T}$ and lnp_s because eq. (2.2.10) is not invertible. Hence the necessity of the 'tweaked Lorenz' grid.

3.2 Is there a best choice of K?

In this section a two-dimensional version ($\partial/\partial y = 0$) of eqs. (2.2.1), (2.2.2), (2.4.11), (2.4.9) and (2.4.6) is integrated with transparent boundary conditions with a view to addressing the question: is there a best choice of missing temperature level, K, for the 'tweaked Lorenz' grid?

Since the above mentioned equations and their transparent boundary conditions are formally the same as those in M06, encoding the σ model involved making only minor changes to the model described there. For the tests discussed in this section the value $T^0 =$ 250K was used. For the discretization, $\Delta x = 10$km, $\Delta t = 9.0$s, $\sigma_{\frac{1}{2}} = 0.001; \sigma_{M+\frac{1}{2}} = 1.0$, $M = 10$ and the levels are equally spaced; thus $\Delta\sigma_m = 0.0999$. The advecting velocity was chosen to be $u_0 = 25\text{ms}^{-1}$. In section 3.4 of M06 extensive tests were performed to estimate the transparency of the boundary conditions. I have repeated the equivalent tests and for the σ model with $K = 5$ and the errors were the same size as those described in M06.

It was shown in M06 the greatest reflection at the boundary is to be expected for the $\{10\}_{\pm}$-wave. (The reflection is proportional to $\bar{u}/c_m$ and c_{10} is the smallest of the gravity wave speeds). Looking at table 2 one concludes that the choice $K = 8$ would give the least reflection. To confirm this the $\{10\}_{+}$-wave exiting experiment (test 3 in section 3 of M06) was performed for the σ model with $K = 2, 5$, and 8. The result was that the

choice $K = 8$ gave the least reflective boundary and $K = 2$ the most reflective boundary. This indicates a procedure for choosing K when using the 'tweaked Lorenz' grid: that associated with the largest value of c_M, because it provides the most transparent boundary condition.

4. The 'tweaked Lorenz' grid and the HIRLAM dynamics.

This sections addresses two questions: (a) Is it difficult to re-program the HIRLAM dynamics on the 'tweaked Lorenz' grid, and (b) is the forecast degraded as a result?

4.1 Program changes

How difficult is it to re-program the HIRLAM model on the 'tweaked Lorenz' grid? The answer is: simple, because the only change to the equations is that eq. (2.24) of the HIRLAM5-5 documentation, Undén et al., 2002, (HIRDOC) becomes

$$\Phi_k = \Phi_s + R_d \sum_{j=k+1}^{N} (\overline{T}_v \Delta lnp)_j + R_d(\alpha \overline{T}_v)_k, \tag{4.1.1}$$

and, by implication, HIRDOC eq. (2.20) becomes

$$G_k = \Phi_s + R_d \sum_{j=k+1}^{N} (\overline{T} \Delta lnp^r)_j + R_d(\alpha^r \overline{T})_k + R_d T^0 lnp_s, \tag{4.1.2}$$

which causes the following changes to HIRDOC eqs. (2.21) and (2.22):

$$\mathbf{G}^{n+1} + \left(\frac{\Delta t_+}{2}\right)\left(\boldsymbol{\gamma}\overline{\boldsymbol{\tau D}} + R_d T^0 \boldsymbol{\nu.D}\right)^{n+1} = \mathbf{H}, \tag{4.1.3}$$

where

$$\mathbf{H} = \Phi_s + \boldsymbol{\gamma}\overline{\boldsymbol{A}}_T + R_d T^0 A_p. \tag{4.1.4}$$

(There is a typographical error in HIRDOC eq. (2.22)).

In all of these equations the 'overline' is defined by eq. (2.4.5). Thus only a few lines of code in the following subroutines need be changed. (a) The definition of $\mathbf{M}$ in IMPINI must be changed to accommodate eq. (4.1.3). In SLDYN, the computation of $\mathbf{\Phi} - \mathbf{G}$ must be changed to use $\overline{T}$ instead of T to accommodate eqs. (4.1.1) and (4.1.2). Similarly for $\mathbf{G}$ in SLDYNM. In SLEXPA, the computation of $\mathbf{H}$ must be changed so that

it uses $\overline{\mathbf{A}}_T$ instead of $\mathbf{A}_T$ to accommodate eq. (4.1.4). In IMPADJ, the computation of $\boldsymbol{\tau D}$ must be changed to a computation of $\overline{\boldsymbol{\tau D}}$ to accommodate eq. (4.1.3).

4.2 Impact on a forecast.

Integrations were performed on a $0.1° \times 0.1°$ horizontal grid. In the vertical the HIRLAM 'reference' 31 hybrid level were used. The time step was 240 seconds. The reference HIRLAM6.2.5 with the upgrades to the semi-Lagrangian described in McDonald (2002) was used. The Norwegian area was chosen. See fig. 3, which shows the starting analysis of sea level pressure over the integration area.

Two 24h forecasts were run. (a) A reference forecast. (b) A repeat forecast using the 'tweaked Lorenz' grid. The level K was chosen to be 18, approximately the 500hpa level. This is well removed from the surface and the tropopause, where the fields are likely to be varying rapidly in the vertical. The outcome was that the latter was just as accurate as the former. See figs. 4 and 5, which show the wind and temperature errors at the 31 model levels after 24h. These are the root mean square errors as measured against the ECMWF validating analysis. As can be seen, switching to the new vertical distribution of the fields does not cause any deterioration of forecast accuracy.

5. **Vertical two grid noise.**

The background to this section is that there was some evidence from FMI of vertical two grid noise in the upper atmosphere in HIRLAM6.2.5. The 'tweaked Lorenz' grid gave rise to the possibility of addressing that problem (see sec. 5.1 below), as did another idea discussed in sec. 5.3 below. Because in subsequent versions of HIRLAM two grid noise in the upper atmosphere ceased to be a problem, work on these ideas was terminated. However, since it is part of the HIRLAMA work plan to address the issue of vertical two grid noise, it may be interesting to resurrect these two ideas in the future, and compare them with other methods of addressing this noise.

5.1 Vertical two grid noise and the spurious mode

In the HIRLAM, and other semi-implicit models which use relaxation boundary conditions, it is interesting that the dynamical equations can be solved without inverting eq. (2.2.10). Is there then, any reason to to worry about the spurious mode associated with the Lorenz grid or can we disregard it as merely a mathematical curiosity? Unfortunately, there is, because it can support a vertical two grid wave, which becomes 'noise' if it attains a large amplitude. This was discussed by Hollingsworth (1995). He pointed out that there is a solution to eq. (2.3.12) for which $\hat{\mathbf{T}}$ has two-grid structure in the vertical even when $\hat{G}$ is smooth in the vertical. The culprit is $\boldsymbol{\gamma}^{-1}$. For example, with ten equally spaced σ levels and with $\sigma_T = 0$, the row sums of $\boldsymbol{\gamma}^{-1}\boldsymbol{I}$ equals (-0.0035,+0.0105,-0.0174,+0.0244,-0.0314,+0.0383,-0.0453, +0.0523,-0.0592,+0.0662). Thus, for example, a $\mathbf{G}$ which is constant in the vertical gives rise to a $\mathbf{T}$ which has two grid structure. The danger is that in the full non-linear system of equations, orographic forcing, or the condensation scheme, for instance, might excite and amplify this spurious solution, making it a possible carrier of noise which has vertical two grid structure. (For the 'tweaked Lorenz' grid with $K = 5$, the row sums of $\check{\boldsymbol{\gamma}}^{-1}\boldsymbol{I}$ equals 3×10^{-9} or less for $m = 1, 10;\ m \neq 5$, in marked contrast to the non-zero oscillating values listed for $\boldsymbol{\gamma}^{-1}\boldsymbol{I}$ above).

5.2 An additional source of vertical noise

It is important to emphasise that there are other solutions to these systems of linear equations which have two grid structure in the vertical. In fact, those associated with c_M are predominantly so; see fig. 2. Thus, eliminating the spurious mode does not exclude all possible vertical two grid structures from these systems of equations.

All of the higher modes are badly distorted by the vertical discretization. For instance, this is true of eigenvectors associated with c_4 to c_{10} inclusive for the 10 level σ model with equally spaced levels; see figs. 1 and 2. This inspires the following idea. Why not 'kill' all (and not just two-grid) the vertical short wavelength waves? They are so inaccurate that they can only be generating noise in the upper levels of the atmosphere. In a semi-implicit integration there is an ideal way to this *and save CPU*: instead of solving Helmholtz equation for $(\mathbf{E}^{-1}\mathbf{D})_{\mathbf{m}}$ for $m = M, M-1, M-2.....$, put them equal to zero.

5.3 Testing

In this section is addressed the question: for how many levels can $(\mathbf{E^{-1}D})_\mathbf{m}$ be put to zero without compromising the accuracy of an integration? The integrations were again performed on same area and with the same data described in sec. 4.2.

Four 24h forecasts were run. (a) A reference forecast. (b) A forecast with $(\mathbf{E^{-1}D})_\mathbf{m}$ set to zero for $m = 27, 31$ prior to transforming back to the physical values of D. (c) The same as (b), but with $m = 22, 31$. (d) The same as (b), but with $m = 17, 31$. Thus, for instance, in forecast (d) the Helmholtz equation was only being solved for 16 of the 31 modes. The outcome is displayed in figs. 6 and 7, which show the wind and temperature errors at the 31 model levels. These are the root mean square errors as measured against the ECMWF validating analysis. As can be seen, even deleting 10 of the $(\mathbf{E^{-1}D})_\mathbf{m}$ has essentially no impact on the forecast errors. (Deleting 15 is a 'bridge too far').

6. Conclusion

The motivation for this work was twofold. Primarily, designing transparent boundary conditions on the Lorenz grid proved to be impossible. Thus, an alternative vertical distribution of the fields was needed. Secondarily that there was evidence for two grid vertical noise in some HIRLAM6.2.5 forecasts, in particular as the number of vertical levels was increased, and I was asked to look for a solution to this problem. The spurious computational mode characteristic of the Lorenz (1960) grid seemed to be a candidate for causing this noise, particularly because 'the increase in vertical resolution tends to increase the amplitude of the computational mode' - Arakawa (1988). In later versions of HIRLAM the evidence for two grid vertical noise disappeared. If it re-appears we can resurrect the ideas discussed here. Of course, the spurious computational mode is also relevant to those interested in initialization, 4dvar, and transparent boundary conditions.

Acknowledgment. Thanks to Isabel Martinez Marco and Jeanette Onvlee for their careful reading of the manuscript and useful suggestion for the improvement thereof.

REFERENCES

Arakawa, A., 1988: Finite difference methods in climate modelling. *Physically based modelling and simulation of climate change, vol. 1*, M. Schlesinger, Ed., D. Reidel, 79-168.

Arakawa, A. and C.S. Konor, 1996: Vertical differencing of the primitive equations based on the Charney-Phillips grid in hybrid σ-p vertical coordinates. *Mon. Wea. Rev.,* **124**, 511-528.

Charney, J.G., and N.A. Phillips, 1953: Numerical integration of the quasigeostrophic equations for barotropic and simple baroclinic flows. *J. Meteor.,* **10**, 71-99.

Daley R., 1979: An application of non-linear normal mode initialization to an operational forecast model. *Atmos. Ocean,* **17**, 97-124 .

Davies, T., et al. 2005: A new dynamical core for the Met Office's global and regional modelling of the atmosphere. *Quart. J. Roy. Meteor. Soc.,* **131**, 1759-1782.

Hollingsworth, A. 1995: A spurious mode in the 'Lorenz' arrangement of Φ and T which does not exist in the 'Charney-Phillips' arrangement. *ECMWF Tech. Memo.,* **211**, 12pp.

Hoskins, B.J., and A.J. Simmons 1975: A multi-layer spectral model and the semi-implicit method. *Quart. J. Roy. Meteor. Soc.,* **101**, 637-655.

Lorenz, E.N., 1960: Energy and numerical weather prediction. *Tellus,* **12**, 364-373.

McDonald, A., 2002: Changes to the HIRLAM needed for finer grids. *HIRLAM newsletter* **42**, 9-17.

McDonald, A., 2006: Transparent lateral boundary conditions for baroclinic waves II. Introducing potential vorticity waves. Tellus, **58A**, 210-220.

Phillips, N.A., 1957: A coordinate system having some special advantages for numerical forecasting. *J. Meteor.* **14**, 184-185.

Undén, P., L. Rontu, H. Järvinen, P. Lynch, J. Calvo, G. Cats, J. Cuxart, K. Eerola, C. Fortelius, J. Antonio García-Moya, C. Jones, G. Lenderlink, A. McDonald, R. McGrath, B. Navascues, N. Woetman Nielsen, V.Ødegaard, E. Rodriguez, M. Rummukainen, R. Rõõm, K. Sattler, B. Hansen Sass, H. Savijärvi, B. Wichers Schreur, R.

Sigg, H. The, A. Tijm, 2002: *HIRLAM-5 Scientific Documentation* 144pp. Available from HIRLAM-5 Project, c/o Per Undén SMHI, S-601 76 Norrköping, SWEDEN

		$Lorenz - grid$		$Charney - Phillips - grid$
$\dot{\sigma}_{\frac{1}{2}}, \sigma_{\frac{1}{2}}$		- - - - - - - - - - - - - -		- - - - - - - - - - - - - -
G_1, u_1, v_1	T_1	———————————		———————————
$\dot{\sigma}_{\frac{3}{2}}, \sigma_{\frac{3}{2}}$		- - - - - - - - - - - - - -	$T_{\frac{3}{2}}$	- - - - - - - - - - - - - -
G_2, u_2, v_2	T_2	———————————		———————————
$\dot{\sigma}_{\frac{5}{2}}, \sigma_{\frac{5}{2}}$		- - - - - - - - - - - - - -	$T_{\frac{5}{2}}$	- - - - - - - - - - - - - -
$\dot{\sigma}_{m-\frac{3}{2}}, \sigma_{m-\frac{3}{2}}$		- - - - - - - - - - - - - -	$T_{m-\frac{3}{2}}$	- - - - - - - - - - - - - -
$G_{m-1}, u_{m-1}, v_{m-1}$	T_{m-1}	———————————		———————————
$\dot{\sigma}_{m-\frac{1}{2}}, \sigma_{m-\frac{1}{2}}$		- - - - - - - - - - - - - -	$T_{m-\frac{1}{2}}$	- - - - - - - - - - - - - -
G_m, u_m, v_m	T_m	———————————		———————————
$\dot{\sigma}_{m+\frac{1}{2}}, \sigma_{m+\frac{1}{2}}$		- - - - - - - - - - - - - -	$T_{m+\frac{1}{2}}$	- - - - - - - - - - - - - -
$\dot{\sigma}_{M-\frac{3}{2}}, \sigma_{M-\frac{3}{2}}$		- - - - - - - - - - - - - -	$T_{M-\frac{3}{2}}$	- - - - - - - - - - - - - -
$G_{M-1}, u_{M-1}, v_{M-1}$	T_{M-1}	———————————		———————————
$\dot{\sigma}_{M-\frac{1}{2}}, \sigma_{M-\frac{1}{2}}$		- - - - - - - - - - - - - -	$T_{M-\frac{1}{2}}$	- - - - - - - - - - - - - -
G_{M-1}, u_M, v_M	T_M	———————————		———————————
$\dot{\sigma}_{M+\frac{1}{2}}, \sigma_{M+\frac{1}{2}}$		- - - - - - - - - - - - - -		- - - - - - - - - - - - - -

TABLE 1. The distribution of the fields over the vertical levels for, on the left, the Lorenz grid, and on the right, the Charney-Phillips grid.

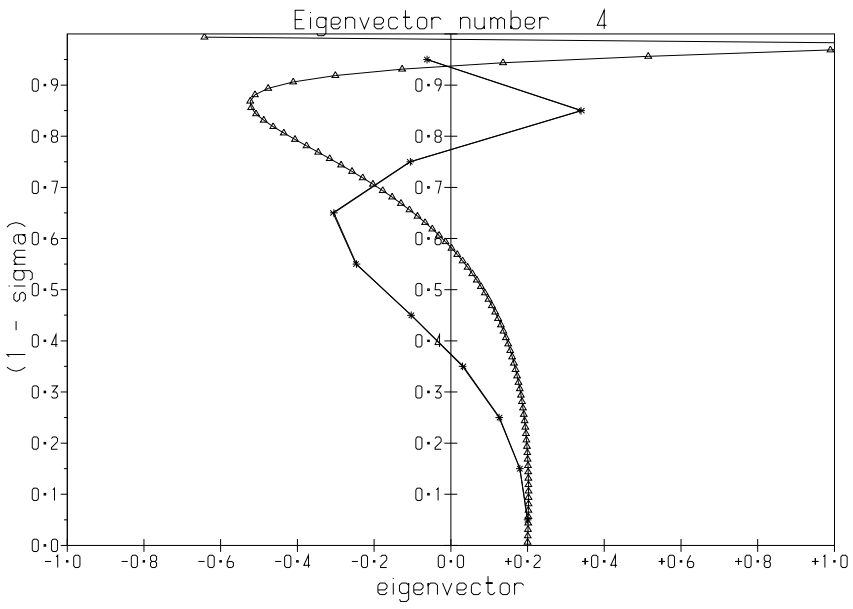

Figure 1: *The eigenvector associated with c_4 plotted with 'triangles' for 80 equally separated σ levels, and with 'pluses' for 10 equally separated σ levels on the Lorenz grid, and with 'exes' for 10 equally separated σ levels on the 'tweaked Lorenz' grid using $K = 8$.*

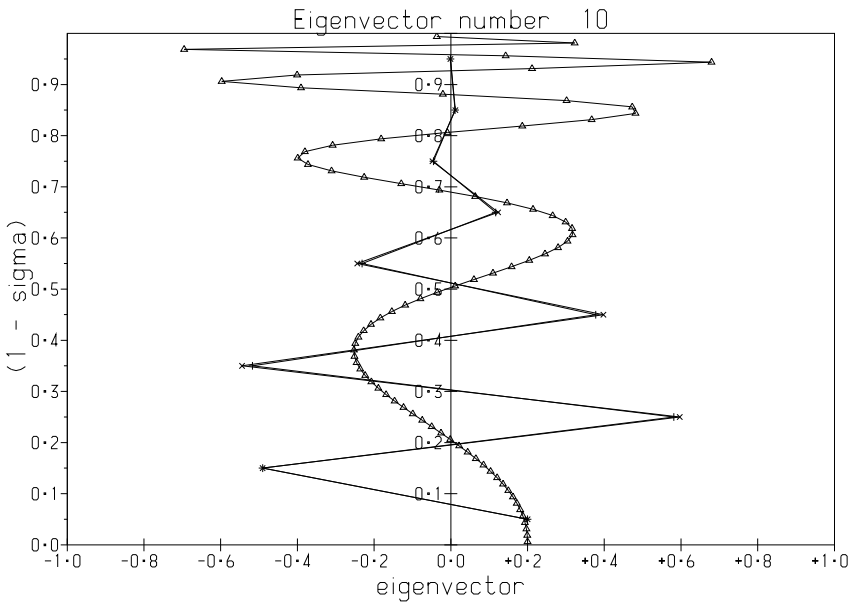

Figure 2: *Same as Fig. 1, but for the eigenvector associated with c_{10}.*

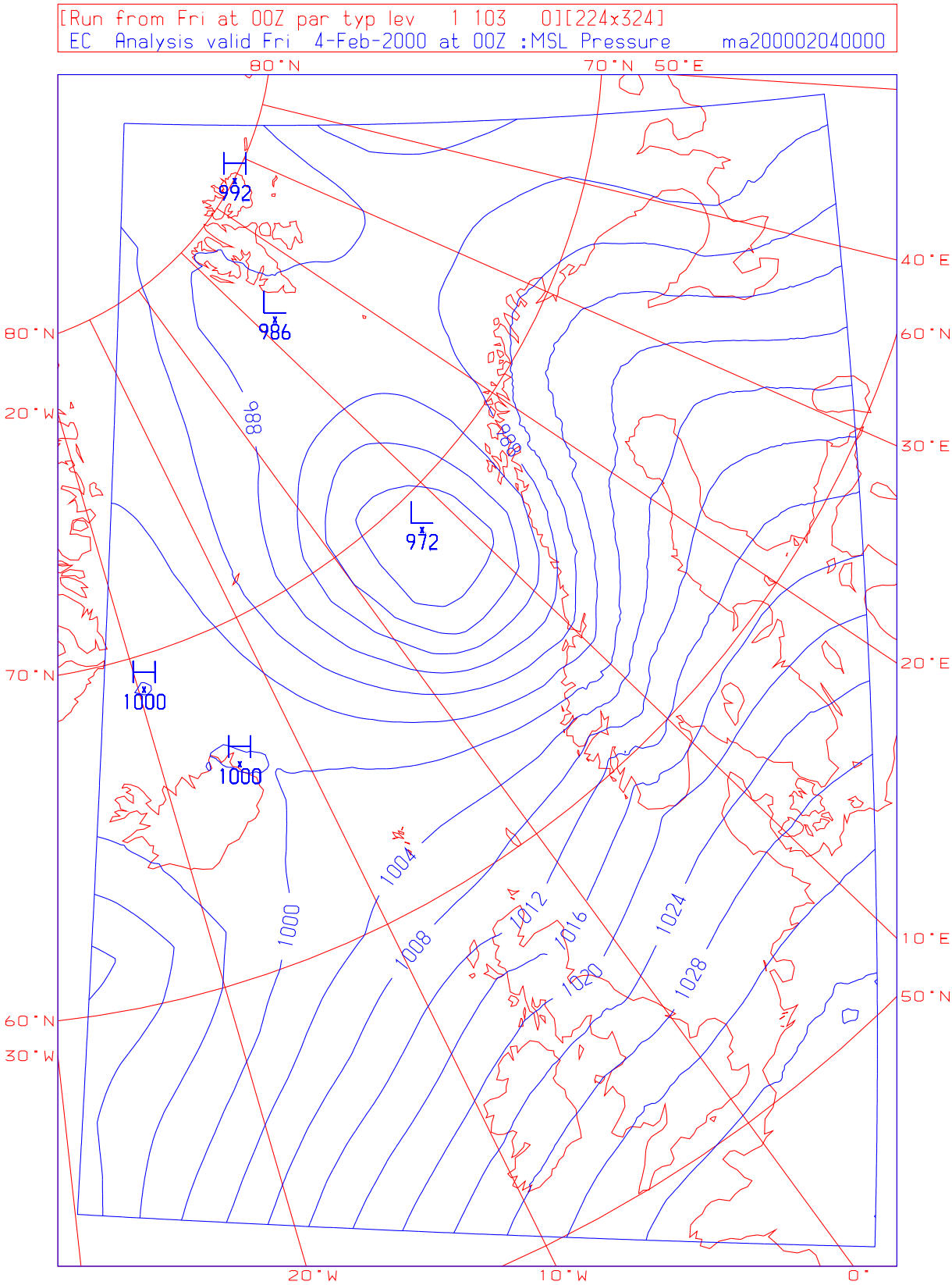

Figure 3: *The starting analysis of sea level pressure.*

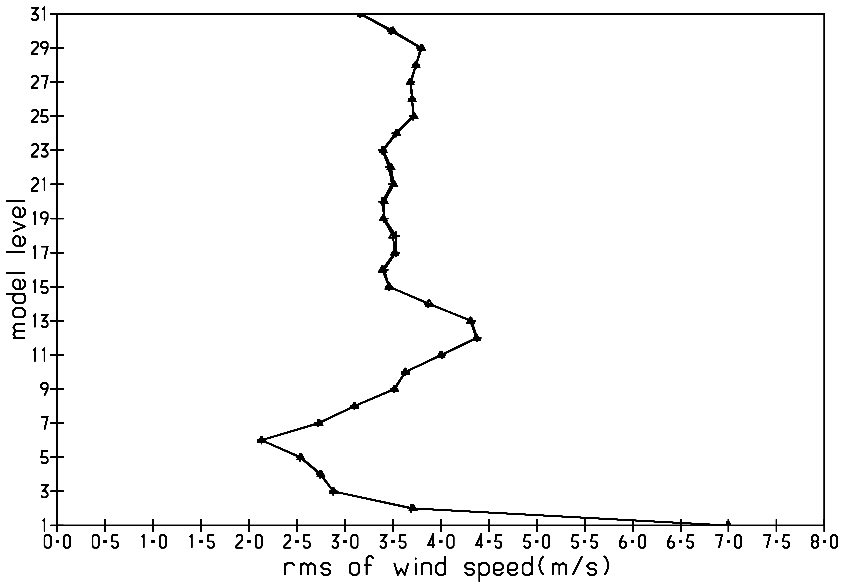

Figure 4: *The root mean square wind errors as measured against the validating ECMWF analysis. The 'triangles' display the errors for the reference forecast; the 'pluses' those for the forecast using the 'tweaked Lorenz' grid.*

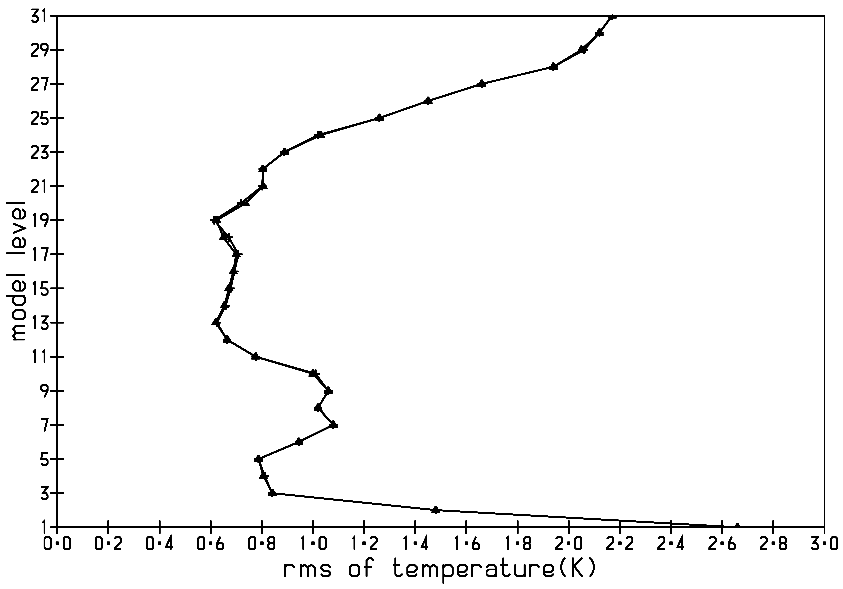

Figure 5: *The same as Fig. 4, except for temperature rather than wind.*

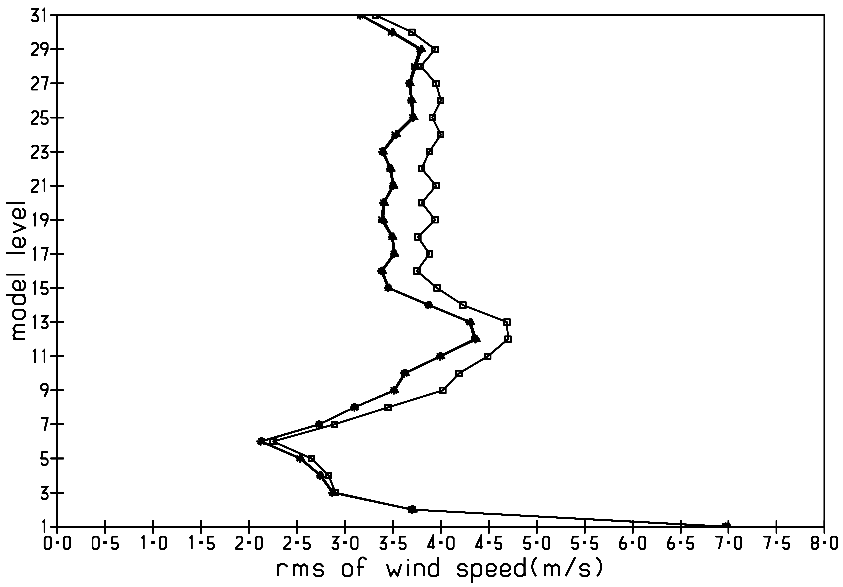

Figure 6: *The root mean square wind errors as measured against the validating ECMWF analysis. The 'triangles' display the errors for the reference forecast(a); the 'pluses' those for forecast(b), (5 D-modes deleted); the 'exes' those for forecast(c), (10 D-modes deleted); the 'squares' those for forecast(d), (15 D-modes deleted).*

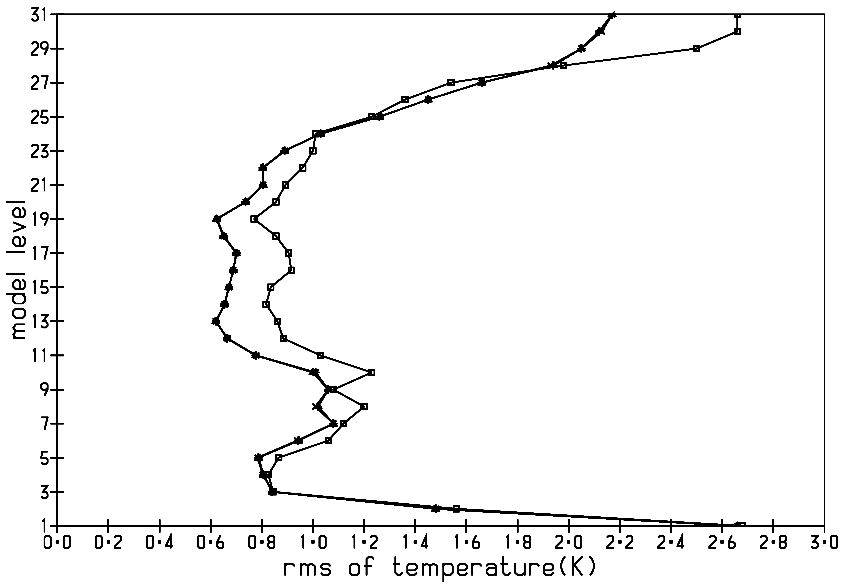

Figure 7: *The same as Fig. 6, except for temperature rather than wind.*